Available online at www.sciencedirect.com
ScienceDirect
International Journal of Heat and Mass Transfer 50 (2007) 1397–1407
International Journal of HEAT and MASS TRANSFER
www.elsevier.com/locate/ijhmt

Analysis of thermal behavior in multi-layer metal thin films based on hyperbolic two-step model

Kuo-Chi Liu *

Department of Mechanical Engineering, Far East University, 49 Chung Hua Road, Hsin-Shih, Tainan 744, Taiwan, ROC

Received 31 March 2006; received in revised form 8 September 2006
Available online 17 November 2006

Abstract

This work theoretically analyzes non-equilibrium thermal behavior in multi-layer metal films with the hyperbolic microscopic two-step model. It is necessary to solve the coupled energy equations or an equation containing higher-order mixed derivatives in both time and space for such problems. The difference in the relaxation times of dissimilar materials introduces the complexity and causes some mathematical difficulties at the interfaces. A numerical scheme is developed in this work and is applied to the examples in double-layer and triple-layer films with an ultrashort pulse heating. To evidence the efficiency of the present numerical scheme, the analytical solutions for the illustrated examples are presented. The effects of the thermal property ratios of dissimilar metals on heat transfer are investigated. It lends the theoretical insight to hyperbolic microscale heat transfer in multi-layer metal films. Results show the difference in the thermal properties of dissimilar materials and the hyperbolic nature of heat transfer in electron gas sufficiently affect the thermal behavior in multi-layer films at early times.

1. Introduction

The multi-layer metal thin-films are widely used for the satisfaction of all mechanical, thermal, and electronic requirements in the development of microelectronics system, photoelectric equipment and microsensors. The advancement of ultrashort pulse laser technologies makes high-rate heating of thin metal films rapidly develop in micromachining, surface hardening, and other applications. However, ultrafast heating on the thin metal films possibly induces thermal damage. Perry et al. [1] presented that ultrashort pulses in the picosecond domain induce thermal damage after the heating pulse is over. Experimental results [2,3] show that thermal damage induced by a sufficiently high-rate heating does not have an obvious signature by excessive temperature. These results further imply that thermal damage can occur in the cold lattices during ultrafast pulse heating on metal films. It is different with that the long-pulse laser heating often drives the heated spot to the melting temperature. For the prevention of thermal damage, the knowledge of ultrafast thermal behavior is demanded.

During the ultrafast heating of thin metal films in the pico/femtosecond domain, the response time of the film is comparable to the phonon–electron thermalization time. Solid lattice and electron gas are not in thermal equilibrium. Classical heat conduction models assuming thermal equilibrium between solid lattice and electron gas lose validity for the prediction of ultrafast thermal behavior. Therefore, the microscale heat transfer models that describe the phenomena of energy interchange between electrons and phonons from a microscopic point of view are proposed for such problems. The parabolic microscopic two-step model has attracted attention in analysis of microscale heat transfer [4–9]. However, as the response time is comparable to or less than the relaxation time, which is the characteristic time for the activation of ballistic behavior in the electron gas, the hyperbolic nature of heat flux carried by electrons is revealed. The parabolic two-step

* Fax: +886 6 597 7510.
E-mail addresses: kuochi.liu@msa.hinet.net, kcliu@cc.feu.edu.tw

0017-9310/$ - see front matter © 2006 Elsevier Ltd. All rights reserved.
doi:10.1016/j.ijheatmasstransfer.2006.09.018

Nomenclature

C	volumetric heat capacity
E	dimensionless heating source, defined as $E = \frac{S\tau_F^{(1)}}{C_e^{(1)}T_0}$
$\widetilde{E}$	Laplace transform of E
G	coupling factor
k	thermal conductivity
ℓ	distance between neighboring nodes
M	total number of layers
N	parameter, defined as $N = \frac{G^{(1)}\tau_F^{(1)}}{C_e^{(1)}}$
Q	dimensionless heat flux, defined as $Q^{(j)} = \frac{q^{(j)}}{T_0\sqrt{k^{(1)}C_e^{(1)}/\tau_F^{(1)}}}$
$\widetilde{Q}$	Laplace transform of Q
q	heat flux
R_c	parameter, defined as $R_c = \frac{C_l^{(1)}}{C_e^{(1)}}$
$R_e^{(j)}$	parameter, defined as $R_e^{(j)} = \frac{C_e^{(j)}}{C_e^{(1)}}$
$R_k^{(j)}$	parameter, defined as $R_k^{(j)} = \frac{k^{(j)}}{k^{(1)}}$
$R_l^{(j)}$	parameter, defined as $R_l^{(j)} = \frac{C_l^{(j)}}{C_l^{(1)}}$
$R_g^{(j)}$	parameter, defined as $R_g^{(j)} = \frac{G^{(j)}}{G^{(1)}}$
$R_t^{(j)}$	parameter, defined as $R_t^{(j)} = \frac{\tau_F^{(j)}}{\tau_F^{(1)}}$
S	heating source
s	Laplace transform parameter
T	temperature
T_0	initial temperature
t	time
V	propagation speed of thermal signal, defined as $V = \sqrt{k/C_e\tau_F}$
x	space coordinate

Greek symbols

β	parameter, defined in Eq. (15)
η	dimensionless space coordinate, defined as $\eta = \frac{x}{\sqrt{k^{(1)}\tau_F^{(1)}/C_e^{(1)}}}$
θ	dimensionless temperature, defined as $\theta = \frac{T-T_0}{T_0}$
$\tilde{\theta}$	Laplace transform of θ
ξ	dimensionless time, defined as $\xi = \frac{t}{\tau_F^{(1)}}$
τ_F	relaxation time at Fermi surface

Superscript

j	layer number

Subscripts

e	electron
i	node number
in	interface
l	lattice
n	number of sub-space domain

model may lose accuracy [10,11]. A reliable microscale heat transfer model must be able to describe the various microstructural interaction effects. Qiu and Tien [10] thus derived the hyperbolic two-step model from the Boltzmann transport equation to account for the hyperbolic nature of heat flux for electrons. The hyperbolic microscopic two-step model is mathematically described with a set of coupled energy equations.

A few works [12–16] for theoretical predictions of the hyperbolic two-step heat conduction problems in the single layer films are available in the literature. Al-Nimr and Arpaci [12] considered that the thermal behavior in thin metal films occurs in two separate stages. The first stage is very short and is described with the hyperbolic two-step model excluding the diffusion term. The second stage is described with the hyperbolic one-step model. Al-Nimr et al. [13] analyzed the distribution of both electron and lattice temperatures in a semiconductor film induced with the application of strong energy pulse. Naji [14] explored the effect of a high frequency fluctuating boundary heating on hyperbolic two-step model. Ref. [15] identifies models that are suitable for describing thermal transport in metal materials heated by a short-pulse laser. Liu [16] have developed some analytical solutions in Laplace transform domain. It is observed from these literatures [12–16] that the solution of the hyperbolic two-step heat conduction problem in a single layer film is difficultly obtained. Due to the complexity and mathematical difficulties induced with the interfacial boundary conditions, the hyperbolic two-step heat conduction problem in multi-layer thin films is more difficult to solve and seems not to be studied. However, there are a few literatures [17–19] for the parabolic two-step problems in multi-layer thin films. The literature [17] shows the large change of temperature gradient at the interface of dissimilar materials. At the same time, Tzou et al. [18] indicate that the ultrafast thermal damage depends on temperature and temperature gradient. As a result, the effect of the hyperbolic nature of heat transfer is worthy to note, because it may induce the discontinuity of the temperature gradient in a heat transfer medium [20–22].

This work will lend the theoretical insight to hyperbolic microscale heat transfer in multi-layer metal films. As Al-Nimr and Arpaci [12] stated, the solution of the coupled energy equations in the microscopic hyperbolic two-step model is difficultly obtained, even after eliminating the coupling, because the resulting equation contains higher-order mixed derivatives in both time and space and leads to complications in the solution procedures. This work develops a numerical scheme for the hyperbolic two-step heat conduc-

tion problem in multi-layer thin films. The Laplace transform technique is used to map the transient problem into steady one. The governing algebraic equations are derived from the continuity of electron temperature and heat flux carried by electrons in conjunction with the approximation functions, which are derived from a corresponding differential equation of the governing equation in the transform domain. The examples in the double-layer and triple-layer films with an ultrashort laser heating described with the Dirac delta function are illustrated. To evidence the accuracy of the present numerical results, a comparison between the present numerical results and the analytical solution is made.

2. Mathematics model

This work considers that the multi-layer metal thin film, as shown in Fig. 1, is heated with an ultrashort pulse laser. The thermal behavior in the metal film is modeled as a one-dimensional problem, if the laser beam diameter is much larger than the heat penetration depth [10,11]. The laser pulse duration is shorter than or comparable to the electron relaxation time. As a result, the hot electrons are not in local thermal equilibrium with the lattice and the hyperbolic energy transport effect on the electron temperature becomes important. Neglecting the thermal dependence of thermal properties, energy conservation equations and the heat flux equation for the hyperbolic microscopic two-step model in layer j are written as [10]

$$C_{\mathrm{e}}^{(j)}\frac{\partial T_{\mathrm{e}}^{(j)}}{\partial t}=-\frac{\partial q^{(j)}}{\partial x}-G(T_{\mathrm{e}}^{(j)}-T_{\mathrm{l}}^{(j)})+S \tag{1a}$$

$$C_{j}^{(j)}\frac{\partial T_{\mathrm{l}}^{(j)}}{\partial t}=G(T_{\mathrm{e}}^{(j)}-T_{\mathrm{l}}^{(j)}) \tag{1b}$$

$$\tau_{\mathrm{F}}^{(j)}\frac{\partial q^{(j)}}{\partial t}+k^{(j)}\frac{\partial T_{\mathrm{e}}^{(j)}}{\partial x}+q^{(j)}=0 \quad \text{for layer } j,\ j=1,\ldots,M \tag{1c}$$

where C is the volumetric heat capacity, G the coupling factor, k the thermal conductivity, q the heat flux, S the radiation heating source, T the temperature, t the time, x the space coordinate, and τ_{F} is the relaxation time at Fermi surface. The subscripts e and l symbol electron and lattice, respectively. Qiu and Tien [10] derived these equations under the assumptions that there is no electrical current during laser heating, the electron gas totally absorbed the incident radiation, and the thermal conductivity is completely contributed with the electron gas. The hyperbolic nature of energy transport by electrons is shown in Eq. (1c). The $\tau_{\mathrm{F}}\frac{\partial q}{\partial t}$ term in Eq. (1c) can be neglected, as the value of the relaxation time τ is small enough, and then Eqs. (1a)–(1c) will become the equations of the parabolic two-step model.

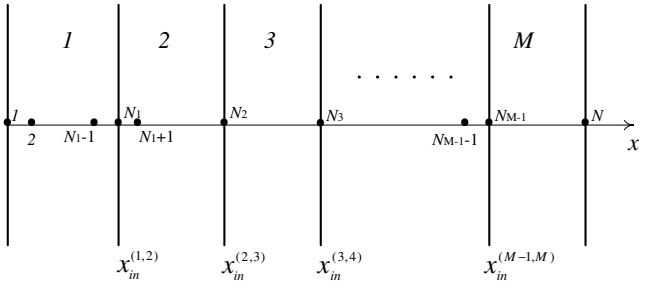

Fig. 1. Schematic diagram of the multi-layer film.

As Qiu and Tien [10] stated, heat losses from the surfaces of the film can be neglected for that the duration of laser heating is very short. Therefore, the boundary conditions at the front and back surfaces are

$$q^{(1)}(0,t)=q^{(M)}(x_N,t)=0 \tag{2}$$

Each layer is assumed to be in perfect thermal contact with the adjacent layers. For the continuity of the electron heat flux and temperature, the boundary conditions at the interface of two layers are

$$q^{(j)}(x_{\mathrm{in}}^{(j,j+1)},t)=q^{(j+1)}(x_{\mathrm{in}}^{(j,j+1)},t) \tag{3a}$$

and

$$T_{\mathrm{e}}^{(j)}(x_{\mathrm{in}}^{(j,j+1)},t)=T_{\mathrm{e}}^{(j+1)}(x_{\mathrm{in}}^{(j,j+1)},t) \tag{3b}$$

where $x_{\mathrm{in}}^{(j,j+1)}$ is the position coordinate of the interface of layer j and layer $j+1$.

Electrons and lattice in the film are assumed to be in thermal equilibrium at the initial status. The initial conditions are

$$T_{\mathrm{e}}^{(j)}(x,0)=T_{\mathrm{l}}^{(j)}(x,0)=T_0 \tag{4a}$$

and

$$q^{(j)}(x,0)=0 \tag{4b}$$

For convenience of statement and analysis, the dimensionless parameters and the thermal property ratios are defined as

$$\theta=\frac{T-T_0}{T_0},\quad \eta=\frac{x}{\sqrt{k^{(1)}\tau_{\mathrm{F}}^{(1)}/C_{\mathrm{e}}^{(1)}}},\quad \xi=\frac{t}{\tau_{\mathrm{F}}^{(1)}},$$

$$Q^{(j)}=\frac{q^{(j)}}{T_0\sqrt{k^{(1)}C_{\mathrm{e}}^{(1)}/\tau_{\mathrm{F}}^{(1)}}},\quad N=\frac{G^{(1)}\tau_{\mathrm{F}}^{(1)}}{C_{\mathrm{e}}^{(1)}},$$

$$R_c=\frac{C_{\mathrm{l}}^{(1)}}{C_{\mathrm{e}}^{(1)}},\quad R_{\mathrm{e}}^{(j)}=\frac{C_{\mathrm{e}}^{(j)}}{C_{\mathrm{e}}^{(1)}},\quad R_k^{(j)}=\frac{k^{(j)}}{k^{(1)}},$$

$$R_{\mathrm{l}}^{(j)}=\frac{C_{\mathrm{l}}^{(j)}}{C_{\mathrm{l}}^{(1)}},\quad R_g^{(j)}=\frac{G^{(j)}}{G^{(1)}},\quad \text{and}\quad R_t^{(j)}=\frac{\tau_{\mathrm{F}}^{(j)}}{\tau_{\mathrm{F}}^{(1)}} \tag{5}$$

Introducing the dimensionless parameters in Eq. (5) into Eqs. (1)–(4) leads to the following dimensionless differential equations of the present problem:

$$R_{\mathrm{e}}^{(j)}\frac{\partial\theta_{\mathrm{e}}^{(j)}}{\partial\xi}=-\frac{\partial Q^{(j)}}{\partial\eta}-NR_g^{(j)}(\theta_{\mathrm{e}}^{(j)}-\theta_{\mathrm{l}}^{(j)})+E \tag{6a}$$

$$R_cR_{\mathrm{l}}^{(j)}\frac{\partial\theta_{\mathrm{l}}^{(j)}}{\partial\xi}=NR_g^{(j)}(\theta_{\mathrm{e}}^{(j)}-\theta_{\mathrm{l}}^{(j)}) \tag{6b}$$

$$R_t^{(j)}\frac{\partial Q^{(j)}}{\partial\xi}+Q^{(j)}=-R_k^{(j)}\frac{\partial\theta_{\mathrm{e}}^{(j)}}{\partial\eta}\quad\text{for layer } j,\ j=1,\ldots,M \tag{6c}$$

subjected to the dimensionless boundary conditions

$$Q^{(1)}(0,\xi)=Q^{(M)}(\eta_N,\xi)=0 \tag{7}$$

$$Q^{(j)}(\eta_{\mathrm{in}}^{(j,j+1)},\xi)=Q^{(j+1)}(\eta_{\mathrm{in}}^{(j,j+1)},\xi) \tag{8a}$$

$$\theta_{\mathrm{e}}^{(j)}(\eta_{\mathrm{in}}^{(j,j+1)},\xi)=\theta_{\mathrm{e}}^{(j+1)}(\eta_{\mathrm{in}}^{(j,j+1)},\xi) \tag{8b}$$

and the initial conditions

$$\theta_{\mathrm{e}}^{(j)}(\eta,0)=\theta_{\mathrm{l}}^{(j)}(\eta,0)=0 \tag{9a}$$

$$Q^{(j)}(\eta,0)=0 \tag{9b}$$

where E is the dimensionless form of the source term S and is defined as $E=S\tau_{\mathrm{F}}^{(1)}/C_{\mathrm{e}}^{(1)}T_0$.

3. Numerical analysis

The Laplace transform technique is used to map the transient problem into the steady one. The Laplace transform of a function $\phi(\xi)$ with respect to ξ is defined as follows:

$$\tilde{\phi}(s)=\int_0^\infty\phi(\xi)\mathrm{e}^{-s\xi}\,\mathrm{d}\xi \tag{10}$$

where s is the Laplace transform parameter.

The dimensionless differential equations (6a)–(6c) and the dimensionless boundary conditions (7), (8a) and (8b) of the present problem are transformed under the initial conditions (9a) and (9b) as

$$\frac{\mathrm{d}\widetilde{Q}^{(j)}}{\mathrm{d}\eta}=-(R_{\mathrm{e}}^{(j)}s+NR_g^{(j)})\tilde{\theta}_{\mathrm{e}}^{(j)}+NR_g^{(j)}\tilde{\theta}_{\mathrm{l}}^{(j)}+\widetilde{E} \tag{11a}$$

$$\tilde{\theta}_{\mathrm{l}}^{(j)}=\frac{NR_g^{(j)}}{R_cR_{\mathrm{l}}^{(j)}s+NR_g^{(j)}}\tilde{\theta}_{\mathrm{e}}^{(j)} \tag{11b}$$

$$\frac{\mathrm{d}\tilde{\theta}_{\mathrm{e}}^{(j)}}{\mathrm{d}\eta}=-\frac{R_t^{(j)}s+1}{R_k^{(j)}}\widetilde{Q}^{(j)}\quad\text{for layer } j,\ j=1,\ldots,M \tag{11c}$$

and

$$\widetilde{Q}^{(1)}(0)=\widetilde{Q}^{(M)}(\eta_N)=0 \tag{12}$$

$$\widetilde{Q}^{(j)}(\eta_{\mathrm{in}}^{(j,j+1)})=\widetilde{Q}^{(j+1)}(\eta_{\mathrm{in}}^{(j,j+1)}) \tag{13a}$$

$$\tilde{\theta}_{\mathrm{e}}^{(j)}(\eta_{\mathrm{in}}^{(j,j+1)})=\tilde{\theta}_{\mathrm{e}}^{(j+1)}(\eta_{\mathrm{in}}^{(j,j+1)}) \tag{13b}$$

Rearrangement of Eqs. (11a)–(11c) leads to the equation

$$\frac{\mathrm{d}^2\tilde{\theta}_{\mathrm{e}}^{(j)}}{\mathrm{d}\eta^2}-\beta^{(j)^2}\tilde{\theta}_{\mathrm{e}}^{(j)}=-\frac{R_t^{(j)}s+1}{R_k^{(j)}}\widetilde{E} \tag{14}$$

where

$$\beta^{(j)^2}=\left[R_{\mathrm{e}}^{(j)}(R_t^{(j)}s^2+s)+R_g^{(j)}N(R_t^{(j)}s+1)-\frac{(R_g^{(j)}N)^2(R_t^{(j)}s+1)}{R_cR_{\mathrm{l}}^{(j)}s+R_g^{(j)}N}\right]\Big/R_k^{(j)} \tag{15}$$

The boundary conditions (12) and (13a) can be rewritten in conjunction with Eq. (11c) as

$$\frac{\mathrm{d}\tilde{\theta}_{\mathrm{e}}^{(1)}(0)}{\mathrm{d}\eta}=0 \tag{16a}$$

$$\frac{R_k^{(j)}}{R_t^{(j)}s+1}\frac{\mathrm{d}\tilde{\theta}_{\mathrm{e}}^{(j)}(\eta_{\mathrm{in}}^{(j,j+1)})}{\mathrm{d}\eta}=\frac{R_k^{(j+1)}}{R_t^{(j+1)}s+1}\frac{\mathrm{d}\tilde{\theta}_{\mathrm{e}}^{(j+1)}(\eta_{\mathrm{in}}^{(j,j+1)})}{\mathrm{d}\eta} \tag{16b}$$

$$\frac{\mathrm{d}\tilde{\theta}_{\mathrm{e}}^{(M)}(\eta_N)}{\mathrm{d}\eta}=0 \tag{16c}$$

For the continuity of the electron heat flux and temperature within layer j, the following conditions are required for the interior nodes in layer j:

$$\tilde{\theta}_{\mathrm{e},n-1}^{(j)}(\eta_i)=\tilde{\theta}_{\mathrm{e},n}^{(j)}(\eta_i) \tag{17}$$

and

$$\frac{\mathrm{d}\tilde{\theta}_{\mathrm{e},n-1}^{(j)}(\eta_i)}{\mathrm{d}\eta}=\frac{\mathrm{d}\tilde{\theta}_{\mathrm{e},n}^{(j)}(\eta_i)}{\mathrm{d}\eta} \tag{18}$$

In order to obtain more accurate numerical results, the derivation of the governing algebraic equations is important. This work plans to derive the governing algebraic equations from Eqs. (17) and (18). In other words, the selection of the approximation functions of $\tilde{\theta}_{\mathrm{e}}$ for the present problem is an important step. The present work determines the approximation function of $\tilde{\theta}_{\mathrm{e}}$ for the sub-space domain n, $[\eta_i,\eta_{i+1}]$, as

$$\tilde{\theta}_{\mathrm{e},n}^{(j)}=A_n\cosh\beta^{(j)}\eta+B_n\sinh\beta^{(j)}\eta+\tilde{P}^{(j)} \tag{19}$$

It is easily observed that Eq. (19) is the analytical solution of Eq. (14) in the sub-space domain $[\eta_i,\eta_{i+1}]$ while the function $\tilde{P}^{(j)}$ is the particular solution of Eq. (14). Therefore, Eq. (19) can be written with the boundary conditions

$$\tilde{\theta}_{\mathrm{e},n}^{(j)}(\eta_i)=\tilde{\theta}_{\mathrm{e},i}^{(j)}\quad\text{and}\quad\tilde{\theta}_{\mathrm{e},n}^{(j)}(\eta_{i+1})=\tilde{\theta}_{\mathrm{e},i+1}^{(j)} \tag{20}$$

as

$$\tilde{\theta}_{\mathrm{e},n}^{(j)}=\frac{1}{\sinh\beta^{(j)}\ell^{(j)}}\Big[\sinh\beta^{(j)}(\eta-\eta_i)(\tilde{\theta}_{\mathrm{e}}-\tilde{P})_{i+1}^{(j)}+\sinh\beta^{(j)}(\eta_{i+1}-\eta)(\tilde{\theta}_{\mathrm{e}}-\tilde{P})_i^{(j)}\Big]+\tilde{P}^{(j)} \tag{21}$$

Similarly, Eq. (19) in the sub-space domain $n-1$, $[\eta_{i-1},\eta_i]$, can be written as

$$\tilde{\theta}_{\mathrm{e},n-1}^{(j)}=\frac{1}{\sinh\beta^{(j)}\ell^{(j)}}\Big[\sinh\beta^{(j)}(\eta-\eta_{i-1})(\tilde{\theta}_{\mathrm{e}}-\tilde{P})_i^{(j)}+\sinh\beta^{(j)}(\eta_i-\eta)(\tilde{\theta}_{\mathrm{e}}-\tilde{P})_{i-1}^{(j)}\Big]+\tilde{P}^{(j)} \tag{22}$$

where ℓ denotes the length of sub-space domain or the distance between two neighboring nodes. The value of ℓ can be different in the different layer. The subscript i is the num-

ber of node. The previous works [20–22] have used the similar approximation functions of temperature in conjunction with the control volume method to discretize the hyperbolic and dual-lag-phase heat conduction equations.

Subsequently, substituting Eqs. (21) and (22) into Eq. (18) and then evaluating the resulting derivative can produce the following discretized form for the interior nodes in layer j as

$$C_{i-1}\tilde{\theta}^{(j)}_{e,i-1} + C_i\tilde{\theta}^{(j)}_{e,i} + C_{i+1}\tilde{\theta}^{(j)}_{e,i+1} = F^{(j)}_i \tag{23}$$

where the coefficients C_{i-1}, C_i, and C_{i+1} are given as

$$C_{i-1} = 1 \tag{24a}$$

$$C_i = -2\cosh(\beta^{(j)}\ell^{(j)}) \tag{24b}$$

$$C_{i+1} = 1 \tag{24c}$$

and the forcing term is given as

$$F^{(j)}_i = \tilde{P}^{(j)}_{i-1} - 2\cosh\beta^{(j)}\ell^{(j)}\tilde{P}^{(j)}_i + \tilde{P}^{(j)}_{i+1} \tag{25}$$

where $\tilde{p}^{(j)}_i = \tilde{P}^{(j)}(\eta_i)$.

The discretized form for the node N_j at the interface of layer j and layer $j+1$ can be produced from Eqs. (16b), (21), and (22) as

$$C_{N_j-1}\tilde{\theta}^{(j)}_{e,N_j-1} + C_{N_j}\tilde{\theta}^{(j,j+1)}_{e,N_j} + C_{N_j+1}\tilde{\theta}^{(j+1)}_{e,N_j+1} = F_{N_j} \tag{26}$$

where

$$C_{N_j-1} = \frac{\beta^{(j)}}{\sinh\beta^{(j)}\ell^{(j)}}\frac{R^{(j)}_k}{R^{(j)}_t s+1} \tag{27a}$$

$$C_{N_j} = -\frac{\beta^{(j)}\cosh\beta^{(j)}\ell^{(j)}}{\sinh\beta^{(j)}\ell^{(j)}}\frac{R^{(j)}_k}{R^{(j)}_t s+1} - \frac{\beta^{(j+1)}\cosh\beta^{(j+1)}\ell^{(j+1)}}{\sinh\beta^{(j+1)}\ell^{(j+1)}}\frac{R^{(j+1)}_k}{R^{(j+1)}_t s+1} \tag{27b}$$

$$C_{N_j+1} = \frac{\beta^{(j+1)}}{\sinh\beta^{(j+1)}\ell^{(j+1)}}\frac{R^{(j+1)}_k}{R^{(j+1)}_t s+1} \tag{27c}$$

and

$$F_{N_j} = C_{N_j-1}\tilde{P}^{(j)}_{N_j-1} + C_{N_j+1}\tilde{P}^{(j+1)}_{N_j+1} - \frac{\beta^{(j)}\cosh\beta^{(j)}\ell^{(j)}}{\sinh\beta^{(j)}\ell^{(j)}}\frac{R^{(j)}_k}{R^{(j)}_t s+1}\tilde{P}^{(j)}_{N_j} - \frac{\beta^{(j+1)}\cosh\beta^{(j+1)}\ell^{(j+1)}}{\sinh\beta^{(j+1)}\ell^{(j+1)}}\frac{R^{(j+1)}_k}{R^{(j+1)}_t s+1}\tilde{P}^{(j+1)}_{N_j} \tag{27d}$$

Rearrangement of Eqs. (23) and (26) with the boundary conditions yields the following matrix equation:

$$[C]\{\tilde{\theta}\} = \{F\} \tag{28}$$

where $[C]$ is a matrix with the complex number s, $\{\tilde{\theta}\}$ is a matrix representing the unknown dimensionless nodal temperatures in the Laplace transform domain, and $\{F\}$ is a matrix representing the forcing term. Thereafter, the application of the Gaussian elimination algorithm and the numerical inversion of the Laplace transform [23] to Eq. (28) can yield the nodal electron temperatures in the physical domain.

And then, the solution of lattice temperature in the Laplce transform domain can be obtained from Eq. (11b). The numerical inversion of the Laplace transform [23] can be applied to perform the inverse transform of $\tilde{\theta}_l$ for θ_l.

4. Illustrative examples

The analysis of thermal behavior in double-layer and triple-layer films induced with an ultrafast laser heating is done. Under the assumption of the incident laser beam evolves all of its energy at dimensionless time $\xi = 0$, the heating duration of ultrafast laser is described by the Dirac delta function $\delta(\xi)$, and then the source term in Eq. (6a) is mathematically described as [24]

$$E = Q_0\exp^{-a\eta}\delta(\xi) \tag{29}$$

where Q_0 is the dimensionless heat flux intensity and a is a constant coefficient. The Laplace transform of E is

$$\tilde{E} = Q_0\exp^{-a\eta} \tag{30}$$

In accordance with Eq. (30), the particular solutions of Eq. (14) in layer j can be expressed as

$$\tilde{P}^{(j)} = \frac{Q_0(R^{(j)}_t s+1)}{R^{(j)}_k(\beta^{(j)^2}-a^2)}\exp(-a\eta) \tag{31}$$

Therefore, the analytical solution of Eq. (14) in layer j is written as

$$\tilde{\theta}^{(j)}_e = A_j\cosh\beta^{(j)}\eta + B_j\sinh\beta^{(j)}\eta + K_j\exp(-a\eta) \tag{32}$$

On the other hand, the analytical solution of $\tilde{\theta}^{(j)}_l$ can be obtained from Eqs. (11b) and (32) as

$$\tilde{\theta}^{(j)}_l = \frac{NR^{(j)}_g}{R_eR^{(j)}_l s + NR^{(j)}_g}[A_j\cosh\beta^{(j)}\eta + B_j\sinh\beta^{(j)}\eta + K_j\exp(-a\eta)] \tag{33}$$

The numerical inversion of the Laplace transform [23] is also applied to perform the inverse transforms of Eqs. (32) and (33) for θ_e and θ_l. The analytical solution is always the best choice to evidence the accuracy of numerical results.

This work performs all the computations with the distance between two neighboring nodes $\ell^{(j)} = 0.02$. The constant values in Eq. (29) are determined as $Q_0 = 5$ and $a = 40$. Table 1 shows thermal properties of common metals at the room temperature.

4.1. For double-layer films

The double-layer film, which is composed with two same thickness films, is considered. The values of $\eta^{(1,2)}_{in}$ and η_N are assumed as 0.5 and 1, respectively. Thus, the boundary conditions (13b) and (16a)–(16c) can be rewritten as

Table 1
Physical constants for metals at the room temperature [25]

	Au	Ag	Cu	Cr	W	Pb
G [TW m^{-3} K^{-1}]	28,000	28,000	48,000	420,000	260,000	120,000
C_e [MJ m^{-3} K^{-1}]	0.021	0.019	0.029	0.058	0.041	0.049
C_l [MJ m^{-3} K^{-1}]	2.5	2.5	3.4	3.2	2.5	1.5
k [W m^{-1} K^{-1}]	317	429	401	93.7	174	35.3
τ_F [ps]	0.04	0.04	0.03	0.003	0.01	0.005

$$\frac{d\tilde{\theta}_e^{(1)}(0)}{d\eta} = 0 \tag{34a}$$

$$\tilde{\theta}_e^{(1)}(0.5) = \tilde{\theta}_e^{(2)}(0.5) \tag{34b}$$

$$\frac{1}{s+1}\frac{d\tilde{\theta}_e^{(1)}(0.5)}{d\eta} = \frac{R_k^{(2)}}{R_t^{(2)}s+1}\frac{d\tilde{\theta}_e^{(2)}(0.5)}{d\eta} \tag{34c}$$

$$\frac{d\tilde{\theta}_e^{(2)}(1)}{d\eta} = 0 \tag{34d}$$

In accordance with the boundary conditions (34a)–(34d), the coefficients in Eqs. (32) and (33) can be written as

$$A_1 = H_1 + H_2A_2 \tag{35a}$$

$$A_2 = (H_3 + H_4)/H_5 \tag{35b}$$

$$B_1 = \frac{aK_1}{\beta^{(1)}} \tag{35c}$$

and

$$B_2 = \frac{aK_2\exp(-a)}{\beta^{(2)}\cosh\beta^{(2)}} - A_2\tanh\beta^{(2)} \tag{35d}$$

where

$$K_1 = \frac{Q_0(s+1)}{\beta^{(1)^2} - a^2} \tag{36a}$$

$$K_2 = \frac{Q_0(R_t^{(2)}s+1)}{R_k^{(2)}(\beta^{(2)^2} - a^2)} \tag{36b}$$

$$H_1 = \left[aK_2\exp(-a)\frac{\sinh\beta^{(2)}/2}{\beta^{(2)}\cosh\beta^{(2)}} - B_1\sinh\frac{\beta^{(1)}}{2} + (K_2 - K_1)\exp(-a/2)\right] \Big/ \cosh\frac{\beta^{(1)}}{2} \tag{36c}$$

$$H_2 = \left(\cosh\frac{\beta^{(2)}}{2} - \sinh\frac{\beta^{(2)}}{2}\tanh\beta^{(2)}\right) \Big/ \cosh\frac{\beta^{(1)}}{2} \tag{36d}$$

$$H_3 = \frac{R_t^{(2)}s+1}{R_k^{(2)}(s+1)}\left[B_1\beta^{(1)}\cosh\frac{\beta^{(1)}}{2} + H_1\beta^{(1)}\sinh\frac{\beta^{(1)}}{2} - aK_1\exp(-a/2)\right] \tag{36e}$$

$$H_4 = aK_2\left[\exp(-a/2) - \exp(-a)\frac{\cosh\beta^{(2)}/2}{\cosh\beta^{(2)}}\right] \tag{36f}$$

and

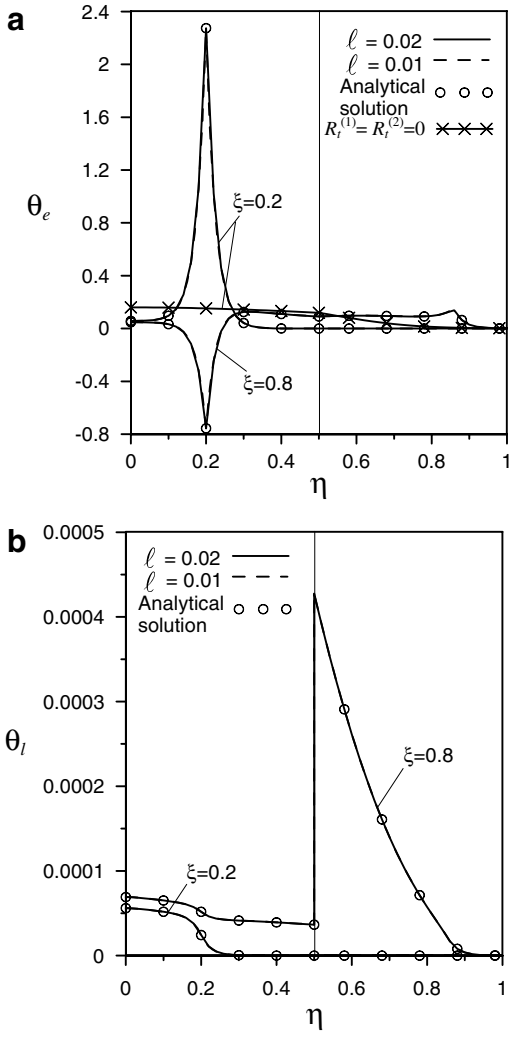

Fig. 2. Distributions of (a) electron and (b) lattice temperatures in a two-layer film with $N = 0.05$, $R_c = 119$, $R_e^{(2)} = 2.762$, $R_k^{(2)} = 0.295$, $R_l^{(2)} = 1.28$, $R_g^{(2)} = 15$, and $R_t^{(2)} = 0.075$ at $\xi = 0.2$ and 0.8.

$$H_5 = \beta^{(2)}\sinh\frac{\beta^{(2)}}{2} - \beta^{(2)}\cosh\frac{\beta^{(2)}}{2}\tanh\beta^{(2)} - \frac{R_t^{(2)}s+1}{R_k^{(2)}(s+1)}H_2\beta^{(1)}\sinh\frac{\beta^{(1)}}{2} \tag{36g}$$

The case of Au–Cr layered film ($N = 0.05$, $R_c = 119$, $R_e^{(2)} = 2.762$, $R_k^{(2)} = 0.295$, $R_l^{(2)} = 1.28$, $R_g^{(2)} = 15$, and $R_t^{(2)} = 0.075$) is first performed and the numerical results are presented in Figs. 2 and 3. Fig. 2 shows the comparison

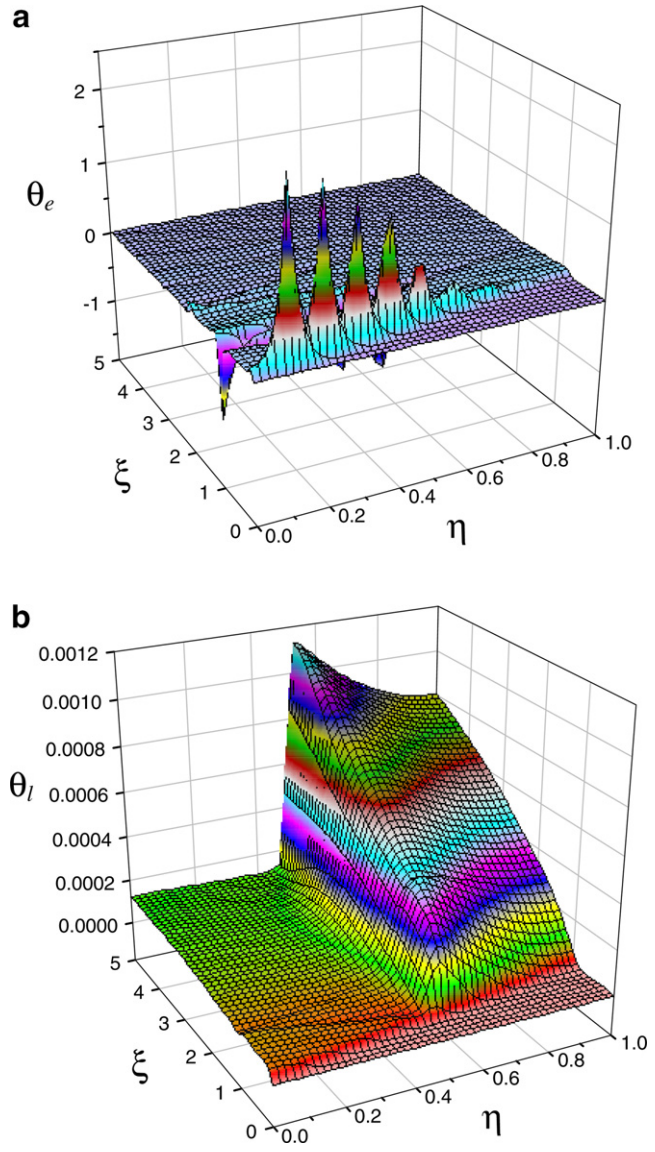

Fig. 3. Distributions of (a) electron and (b) lattice temperatures in the space and time domains for the two-layer film with $N = 0.05$, $R_c = 119$, $R_e^{(2)} = 2.762$, $R_k^{(2)} = 0.295$, $R_l^{(2)} = 1.28$, $R_g^{(2)} = 15$, and $R_t^{(2)} = 0.075$, computed with the time interval $\Delta\xi = 0.1$.

between the present numerical results computed with $\ell^{(j)} = 0.01$ and 0.02 and the analytical solution at $\xi = 0.2$ and 0.8. It is found that the present numerical results for the distributions of electron and lattice temperatures agree with the analytical solution. This implies the present numerical results are accurate and reliable for such problems. Referring to Eq. (29), the location of the energy pulse peak is at $\eta = 0.0$ for $\xi = 0$. It is observed from Fig. 2(a) that the energy pulse peak moves to $\eta = 0.2$ at $\xi = 0.2$ and the region before the energy pulse is not disturbed. This phenomenon shows that heat transfer proceeds in a finite velocity. In accordance with the definition of η and ξ, the propagation velocity of thermal pulse in electron gas can be stated as $V_1 = \sqrt{k^{(1)}/C_e^{(1)}\tau^{(1)}}$ within layer 1 [10]. As $\xi = 0.8$, the energy pulse has encountered the interface between two layers. The transmission-reflection phenomenon is created at the interface due to the difference in the thermal properties of dissimilar materials. A part of energy gets across the interface into layer 2, the other part is reflected and moves toward the boundary surface $\eta = 0$. Because the propagation velocity of thermal pulse in electron gas in layer 2 becomes $V_2 = \sqrt{R_k^{(2)}/R_e^{(2)}R_t^{(2)}}V_1$, the location of the transmitted pulse peak is over $\eta = 0.8$ for $R_e^{(2)} = 2.762$, $R_k^{(2)} = 0.295$, and $R_t^{(2)} = 0.075$ at $\xi = 0.8$. The higher velocity of heat transfer in layer 2 makes more energy across the interface and creates a downward reflected thermal pulse. On the other hand, heat energy transfers into the lattice and raises the lattice temperature through the phonon–electron interactions, as shown in Fig. 2(b). The heat-affected region in lattice is the same with that in electron gas. However, the negative value does not appear in the lattice temperature distribution for the downward reflected pulse in electron gas at $\xi = 0.8$. At the interface $\eta = 0.5$, the lattice temperature distribution drastically increase and a clear discontinuity of the temperature gradient is developed for $\xi = 0.8$. This behavior is similar to that based on the parabolic two-step model [17,18]. But, the lattice temperature does not increase in a uniform form in layer 1 from $\xi = 0.2$ to $\xi = 0.8$. In addition, the thermal behavior for $R_t^{(1)} = R_t^{(2)} = 0.0$ can be described with the parabolic two-step model. It is obvious that the parabolic two-step thermal behavior is different with the hyperbolic thermal behavior.

Fig. 3 presents the distributions of electron and lattice temperatures in the space and time domains for the case of $N = 0.05$, $R_c = 119$, $R_e^{(2)} = 2.762$, $R_k^{(2)} = 0.295$, $R_l^{(2)} = 1.28$, $R_g^{(2)} = 15$, and $R_t^{(2)} = 0.075$. Fig. 3(a) displays that the original structure of energy pulse carried by electrons and the transmission-reflection phenomenon at the interface gradually decay with time increasing, due to the phonon–electron interactions and heat diffusion. $C_e^{(2)} = 2.762C_e^{(1)}$ for $R_e^{(2)} = 2.762$ means that the ability of energy absorption of electron gas in layer 2 is larger than that in layer 1. The decay speed of thermal pulse in layer 2 is faster than that in layer 1. Thermal pulses travel back and forth at a finite propagation speed for the hyperbolic nature of energy transport, and the negative solutions are predicted [20–22]. It is found from Fig. 3(b) that the lattice temperature increases with time increasing for the phonon–electron interactions and the discontinuity of the temperature gradient exists at the interface during $0 \leqslant \xi \leqslant 5$. It is known that $R_l^{(2)}$ is the volumetric lattice heat capacity ratio between layers 1 and 2. As the value of $R_l^{(2)}$ increases, the value of C_l in layer 2 increases or the value of C_l in layer 1 decreases. In other words, the lattice of layer 2 can accumulate more energy than the lattice of layer 1. As a result, the lattice temperature in layer 2 should be in a relatively low value for the larger value of $R_l^{(2)}$. However, due to the larger value of couple factor between electrons and phonons, the effect of the phonon–electron interactions gets stronger in layer 2. Thus the lattice temperature in layer 2 is higher

than that in layer 1 for $R_g^{(2)} = 15$, even $R_l^{(2)} = 1.28$, as shown in Fig. 3(b). It is worthy to note that all lattice temperature distributions during $0 \leqslant \xi \leqslant 5$ are in the positive domain, though some electron temperature distributions are in the negative domain for the difference in the thermal properties of dissimilar materials and the transmission-reflection phenomenon at the interface.

To further know the effects of the difference in the thermal properties of dissimilar materials on the temperature distribution, the second case, Cr–Au layered film ($N = 0.02$, $R_c = 55.17$, $R_e^{(2)} = 0.362$, $R_k^{(2)} = 3.383$, $R_l^{(2)} = 0.78$, $R_g^{(2)} = 0.067$), and $R_t^{(2)} = 13.33$, is studied in this part. The numerical results for $\xi = 0.2$ and 0.8 are presented in Fig. 4. The present results are also in a good agreement with the analytical solution. As $\xi = 0.2$, the energy pulse has not reached the interface yet. Layer 2 does not affect the distributions of electron and lattice temperatures. The distributions of electron and lattice temperatures shown in Fig. 4 for $\xi = 0.2$ are the same with those in Fig. 2 under that layer 1 is the reference layer. As $\xi = 0.8$, the energy pulse has encountered the interface and the transmission-reflection phenomenon happens. It is found from Fig. 4 and the definition of $\eta$and ξthat the displacement of energy pulse in film can be described with tV. For $R_e^{(2)} = 0.362$, $R_k^{(2)} = 3.383$, and $R_t^{(2)} = 13.33$, the velocity of heat transfer in layer 2 is slower than that in layer 1. Fig. 4(a) shows an upward reflected thermal pulse and the most energy accumulates in layer 1 for $R_e^{(2)} = 0.362$ and $R_l^{(2)} = 0.78$ at $\xi = 0.8$. As $R_g^{(2)} = 0.067$, the phonon–electron interactions in layer 2 are weaker than that in layer 1. That is why the lattice temperature in layer 2 is further lower than that in layer 1 at $\xi = 0.8$. The comparison between Figs. 2 and 4 further shows the difference in the thermal properties of dissimilar materials can affect the temperature distribution and the temperature gradient.

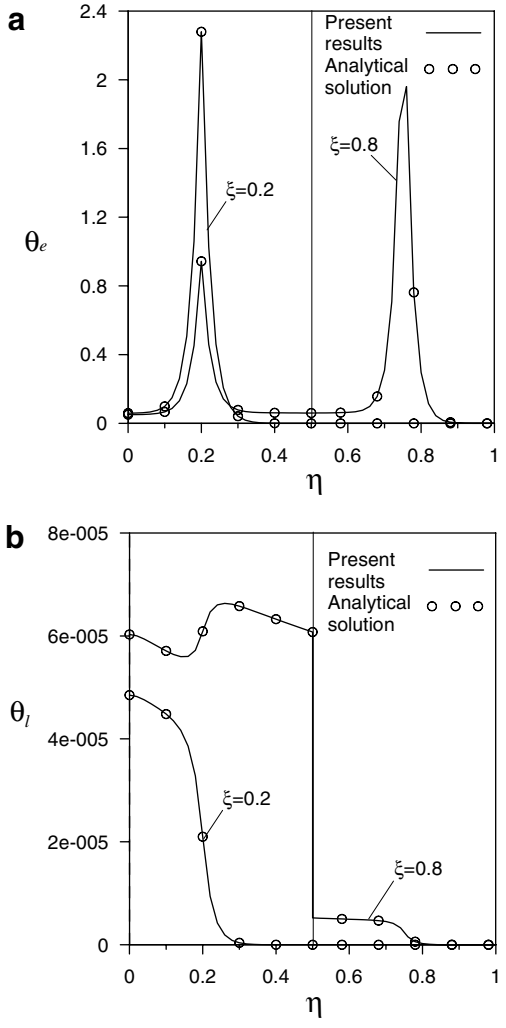

Fig. 4. Distributions of (a) electron and (b) lattice temperatures in a two-layer film with $N = 0.02$, $R_c = 55.17$, $R_e^{(2)} = 0.362$, $R_k^{(2)} = 3.383$, $R_l^{(2)} = 0.78$, $R_g^{(2)} = 0.067$, and $R_t^{(2)} = 13.33$ at $\xi = 0.2$ and 0.8.

4.2. For triple-layer film

This work pays attention on a triple-layer film of $\eta_{in}^{(1,2)} = 0.3$, $\eta_{in}^{(2,3)} = 0.7$, and $\eta_N = 1$. The boundary conditions (13b) and (16a)–(16c) are rewritten as

$$\frac{d\tilde{\theta}_e^{(1)}(0)}{d\eta} = 0 \tag{37a}$$

$$\tilde{\theta}_e^{(1)}(0.3) = \tilde{\theta}_e^{(2)}(0.3) \tag{37b}$$

$$\frac{1}{s+1}\frac{d\tilde{\theta}_e^{(1)}(0.3)}{d\eta} = \frac{R_k^{(2)}}{R_t^{(2)}s+1}\frac{d\tilde{\theta}_e^{(2)}(0.3)}{d\eta} \tag{37c}$$

$$\tilde{\theta}_e^{(2)}(0.7) = \tilde{\theta}_e^{(3)}(0.7) \tag{37d}$$

$$\frac{R_k^{(2)}}{R_t^{(2)}s+1}\frac{d\tilde{\theta}_e^{(2)}(0.7)}{d\eta} = \frac{R_k^{(3)}}{R_t^{(3)}s+1}\frac{d\tilde{\theta}_e^{(3)}(0.7)}{d\eta} \tag{37e}$$

$$\frac{d\tilde{\theta}_e^{(3)}(1)}{d\eta} = 0 \tag{37f}$$

The coefficients in Eqs. (32) and (33) are obtained from the boundary conditions (37a)–(37f) and are written as

$$A_1 = A_2\frac{\cosh 0.3\beta^{(2)}}{\cosh 0.3\beta^{(1)}} + B_2\frac{\sinh 0.3\beta^{(2)}}{\cosh 0.3\beta^{(1)}} + \frac{\exp(-0.3a)}{\cosh 0.3\beta^{(1)}}(K_2 - K_1) - B_1\tanh 0.3\beta^{(1)} \tag{38a}$$

$$A_2 = (H2B_1 + H3H5A_3 + H3H6 + H4)/H1 \tag{38b}$$

$$A_3 = (H7 - H8)/(H9 - H10) \tag{38c}$$

$$B_1 = \frac{aK_1}{\beta^{(1)}} \tag{38d}$$

$$B_2 = H5A_3 + H6 \tag{38e}$$

and

$$B_3 = \frac{aK_3\exp(-a)}{\beta^{(3)}\cosh\beta^{(3)}} - A_3\tanh\beta^{(3)} \tag{38f}$$

where

$$H1=\frac{R_k^{(2)}(s+1)}{R_t^{(2)}s+1}\beta^{(2)}\sinh 0.3\beta^{(2)}-\beta^{(1)}\tanh 0.3\beta^{(1)}\cosh 0.3\beta^{(2)} \tag{39a}$$

$$H2=\beta^{(1)}\cosh 0.3\beta^{(1)}-\beta^{(1)}\tanh 0.3\beta^{(1)}\sinh 0.3\beta^{(1)} \tag{39b}$$

$$H3=\beta^{(1)}\tanh 0.3\beta^{(1)}\sinh 0.3\beta^{(2)}-\frac{R_k^{(2)}(s+1)}{R_t^{(2)}s+1}\beta^{(2)}\cosh 0.3\beta^{(2)} \tag{39c}$$

$$H4=\left[\beta^{(1)}(K_2-K_1)\tanh 0.3\beta^{(1)}+a\left(\frac{R_k^{(2)}(s+1)}{R_t^{(2)}s+1}K_2-K_1\right)\right]\exp(-0.3a) \tag{39d}$$

$$H5=\frac{(\cosh 0.7\beta^{(3)}-\sinh 0.7\beta^{(3)}\tanh\beta^{(3)})H1}{H3\cosh 0.7\beta^{(2)}+H1\sinh 0.7\beta^{(2)}} \tag{39e}$$

$$H6=\frac{\left[\sinh 0.7\beta^{(3)}\frac{aK_3\exp(-a)}{\beta^{(3)}\cosh\beta^{(3)}}+(K_3-K_2)\exp(-0.7a)\right]H1-\cosh 0.7\beta^{(2)}(H2B_1+H4)}{H3\cosh 0.7\beta^{(2)}+H1\sinh 0.7\beta^{(2)}} \tag{39f}$$

$$H7=\frac{(H2B_1+H3H6+H4)}{H1}\beta^{(2)}\sinh 0.7\beta^{(2)}+H6\beta^{(2)}\cosh 0.7\beta^{(2)}-aK_2\exp(-0.7a) \tag{39g}$$

$$H8=\frac{R_k^{(3)}(R_t^{(2)}s+1)}{R_k^{(2)}(R_t^{(3)}s+1)}\left(\frac{\cosh 0.7\beta^{(3)}}{\cosh\beta^{(3)}}aK_3\exp(-a)-aK_3\exp(-0.7a)\right) \tag{39h}$$

$$H9=\frac{R_k^{(3)}(R_t^{(2)}s+1)}{R_k^{(2)}(R_t^{(3)}s+1)}(\beta^{(3)}\sinh 0.7\beta^{(3)}-\beta^{(3)}\cosh 0.7\beta^{(3)}\tanh\beta^{(3)}) \tag{39i}$$

and

$$H10=H5\beta^{(2)}\cosh 0.7\beta^{(2)}+\frac{H3H5}{H1}\beta^{(2)}\sinh 0.7\beta^{(2)} \tag{39j}$$

It is found from the above Eqs. (38a)–(38f), (39a)–(39j) that the analytical solution for the triple-layer film becomes complicate. It implies that the difficulty for solving such problems increases with the composite interfaces of dissimilar materials increasing.

The numerical results shown in Figs. 5 and 6 are computed for a Au–Cr–Au layered film with $N=0.05$, $R_c=119$, $R_e^{(2)}=2.762$, $R_k^{(2)}=0.295$, $R_l^{(2)}=1.28$, $R_g^{(2)}=15$, $R_t^{(2)}=0.075$, and $R_e^{(3)}=R_k^{(3)}=R_l^{(3)}=R_g^{(3)}=R_t^{(3)}=1$. Solving the present problems may encounter some mathematical difficulties that must be precluded for obtaining an admissible solution. The mathematical difficulties may arise when a thermal pulse encounters a boundary or another temperature discontinuity. Due to composite interface increasing, the analysis of the present example is more difficult. However, Fig. 5 shows a good agreement of the present results with the analytical solution. It further displays the efficiency of the present numerical scheme for such problems. Fig. 5(a) shows a downward reflected thermal pulse in electron gas is created at the interface $\eta=\eta_{in}^{(1,2)}=0.3$ and moves in layer 1 for the reasons corresponding to Fig. 2(a). As $\xi=0.8$, this reflected thermal pulse has encountered the boundary surface $\eta=0$ and moves toward the interface $\eta=\eta_{in}^{(1,2)}=0.3$. At the same time, the transmitted thermal pulse has encountered the interface $\eta=\eta_{in}^{(2,3)}=0.7$. Another transmission-reflection phenomenon happens in layers 2 and 3. It is observed that multi thermal pulses appear at the same time for the effects of the transmission-reflection at the interfaces of dissimilar materials. The temperature gradient is obvious around the thermal pulses. Due to superposition of thermal pulses, heat diffusion, and the phonon–electron interactions, the thermal pulses have faded at $\xi=1.2$. On the other hand, there no obvious thermal pulse exists in lattice, as shown in Fig. 5(b). But, the lattice temperature distributions in

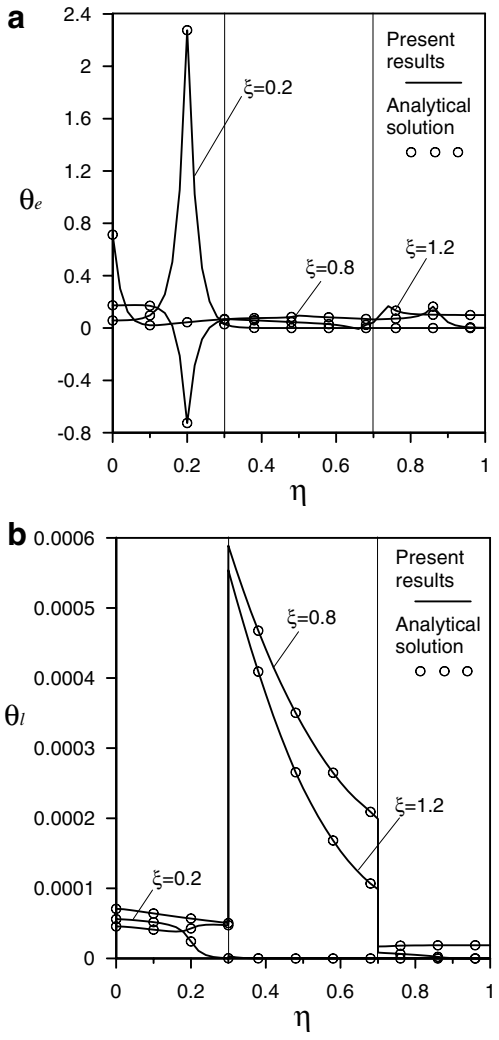

Fig. 5. Distributions of (a) electron and (b) lattice temperatures in a triple-layer film with $N=0.05$, $R_c=119$, $R_e^{(2)}=2.762$, $R_k^{(2)}=0.295$, $R_l^{(2)}=1.28$, $R_g^{(2)}=15$, $R_t^{(2)}=0.075$, and $R_e^{(3)}=R_k^{(3)}=R_l^{(3)}=R_g^{(3)}=R_t^{(3)}=1$ for various ξ values.

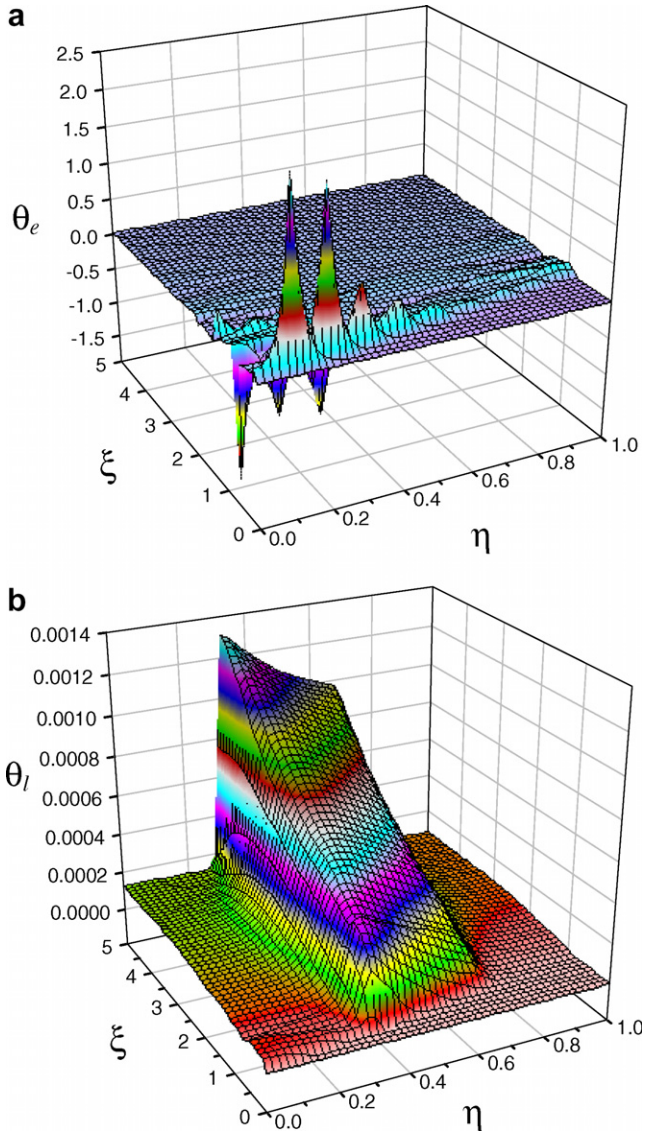

Fig. 6. Distributions of (a) electron and (b) lattice temperatures in the space and time domains for the triple-layer film with $N = 0.05$, $R_c = 119$, $R_e^{(2)} = 2.762$, $R_k^{(2)} = 0.295$, $R_l^{(2)} = 1.28$, $R_g^{(2)} = 15$, $R_t^{(2)} = 0.075$, and $R_e^{(3)} = R_k^{(3)} = R_l^{(3)} = R_g^{(3)} = R_t^{(3)} = 1$, computed with the time interval $\Delta\xi = 0.1$.

layer 2 are sharper than that in layers 1 and 3. This result implies that the lattice temperature gradient depends on the thermal properties of material. The comparison among Figs. 2, 4, and 5 also implies that the thermal property ratios of dissimilar materials can affect the temperature distribution and the temperature gradient in layered films. In other words, the heating direction may change the temperature distributions and the temperature gradient in layered films.

The distributions of electron and lattice temperatures in the space and time domains for the triple-layer film are displayed in Fig. 6. It is found from Fig. 6(a) that the thermal pulses concentrates in layer 1 for the effects of the thermal properties in layer 2. Heat energy carried by electrons is rapidly transferred to lattice through the phonon–electron interactions for $R_g^{(2)} = 15$ in layer 2. The thermal pulses transmitted in electron gas go to decay in layer 2. Fig. 6(b) shows that the lattice temperature in layer 2 is higher than that in layer 1. This result is similar to that shown in Fig. 3(b). And also, the negative solutions appear in Fig. 6(a) for the same reason illustrated for Fig. 3(a).

5. Conclusions

This work analyzes the microscopic heat transfer in multi-layer metal films with the hyperbolic two-step model, and an efficient numerical scheme is developed to counter the mathematical difficulties induced by the hyperbolic nature of heat transfer in electron gas, the coupled energy equations, and the interfacial boundary conditions. The numerical results and analytical solutions are presented for the problems in the double-layer and triple-layer films with an ultrashort laser heating, which the pulse duration is described with the Dirac delta function. The comparison between the numerical results and the analytical solutions evidences the efficiency of the present numerical scheme for such problems. Results show that thermal pulses travel back and forth in electron gas at a finite propagation speed for the hyperbolic nature of energy transport. However, the effect of the hyperbolic nature of heat transfer on the lattice temperature distribution is not obvious. The heat-affected region depends on the propagation velocity of heat transfer. The difference in the thermal properties of dissimilar materials creates the transmission-reflection phenomenon of thermal pulse at the interface and affects the temperature distribution and the temperature gradient in layered films. The thermal pulses in electron gas fade for superposition of thermal pulses, heat diffusion, and the phonon–electron interactions.

Acknowledgement

Support for this work by the National Science Counsel of the Republic of China under Grant No. 94-2212-E-269-012 is gratefully acknowledged.

References

[1] M.D. Perry, B.C. Staurt, P.S. Bank, M.D. Feit, V. Yanovsky, A.M. Rubenchik, Ultrashort-pulse laser machining of dielectric materials, J. Appl. Phys. 85 (1999) 6803–6810.
[2] C. Momma, S. Nolte, B.N. Chichkov, F.V. Alvensleben, A. Tunnermann, Precise laser ablation with ultrashort pulses, Appl. Surf. Sci. 109 (1997) 15–19.
[3] M.D. Shirk, P.A. Molian, A review of ultrashort pulsed laser ablation of materials, J. Laser Appl. 10 (1998) 18–28.
[4] H.E. Elsayed-Ali, T.B. Norris, M.A. Pessot, G.A. Mourou, Time-resolved observation of electron–phonon relaxation in copper, Phys. Rev. Lett. 58 (12) (1987) 1212–1215.
[5] T.Q. Qiu, C.L. Tien, Short-pulse laser heating on metals, Int. J. Heat Mass Transfer 35 (1992) 719–726.
[6] M.A. Al-Nimr, S. Kiwan, Effect of thermal losses on the microscopic two-step heat conduction model, Int. J. Heat Mass Transfer 44 (2001) 1013–1018.

[7] M.A. Al-Nimr, M. Hader, M. Naji, Use of the microscopic parabolic heat conduction model in place of the macroscopic model validation criterion under harmonic boundary heating, Int. J. Heat Mass Transfer 46 (2003) 333–339.
[8] I.H. Chowdhury, X. Xu, Heat transfer in femtosecond laser processing of metal, Numer. Heat Transfer, Part A 44 (2003) 219–232.
[9] B. Barron, W. Dal, A hybrid FE–FD scheme for solving parabolic two-step micro heat transfer equations in an irregularly shaped three-dimensional double-layered thin film, Numer. Heat Transfer, Part B 49 (2006) 437–465.
[10] T.Q. Qiu, C.L. Tien, Heat transfer mechanism during short-pulse laser heating of metals, J. Heat Transfer 115 (1993) 835–841.
[11] D.Y. Tzou, The generalized lagging response in small-scale and high-rate heating, Int. J. Heat Mass Transfer 38 (1995) 3231–3240.
[12] M.A. Al-Nimr, V.S. Arpaci, The thermal behavior of thin metal films in the hyperbolic two-step model, Int. J. Heat Mass Transfer 43 (2000) 2021–2028.
[13] M.A. Al-Nimr, O.M. Haddad, V.S. Arpaci, Thermal behaviour of metal films – a hyperbolic two-step model, Heat Mass Transfer 35 (1999) 459–464.
[14] M. Naji, M.A. Al-Nimr, M. Hader, The validity of using the microscopic hyperbolic heat conduction model under a harmonic fluctuating boundary heating source, Int. J. Thermophys. 24 (2003) 545–557.
[15] J.K. Chen, J.E. Beraun, C.L. Tham, Investigation of thermal response caused by pulse laser heating, Numer. Heat Transfer, Part A 44 (2003) 705–722.
[16] K.C. Liu, Analysis for microscopic hyperbolic two-step heat transfer problems, Int. J. Thermophys. 27 (2006) 596–613.
[17] T.Q. Qiu, C.L. Tien, Femtosecond laser heating of multilayered metals – I. Analysis, Int. J. Heat Mass Transfer 37 (17) (1994) 2789–2797.
[18] D.Y. Tzou, J.K. Chen, J.E. Beraun, Hot-electron blast induced by ultrashort-pulsed lasers in layered media, Int. J. Heat Mass Transfer 45 (2002) 3369–3382.
[19] M.G. Ibrahim Wael, H.E. Elisayed-Ali, C.E. Bonner Jr., M. Shinn, Ultrafast investigation of electron dynamics in multi-layer metals, Int. J. Heat Mass Transfer 47 (2004) 2261–2268.
[20] H.T. Chen, K.C. Liu, Study of hyperbolic heat conduction problem in the film and substrate composite with the interface resistance, Jpn. J. Appl. Phys. 41 (2002) 6267–6275.
[21] K.C. Liu, H.T. Chen, Numerical analysis for the hyperbolic heat conduction problem under a pulsed surface disturbance, Appl. Math. Comput. 159 (2004) 887–901.
[22] K.C. Liu, Analysis of dual-phase-lag thermal behavior in layered films with temperature-dependent interface thermal resistance, J. Phys. D: Appl. Phys. 38 (2005) 3722–3732.
[23] G. Honig, U. Hirdes, Study of hyperbolic heat conduction problem in the film and substrate composite with the interface resistance, J. Comput. Appl. Math. 9 (1984) 113–132.
[24] M.A. Al-Nimr, V.S. Arpaci, Picosecond thermal pulses in thin metal films, J. Appl. Phys. 85 (1999) 2517–2521.
[25] K.J. Hays-Stang, A. Haji-Sheikh, A unified solution for heat conduction in thin films, Int. J. Heat Mass Transfer 42 (1999) 455–465.